

## Properties of a relativistic equation of state for collapse-driven supernovae

K. Sumiyoshi<sup>a,1</sup>, H. Suzuki<sup>b,2</sup>, S. Yamada<sup>c,3</sup>, and H. Toki<sup>d,4</sup>

<sup>a</sup>Numazu College of Technology,

Ooka 3600, Numazu, Shizuoka 410-8501, Japan

<sup>b</sup>Faculty of Science and Technology, Tokyo University of Science,

Yamazaki 2641, Noda, Chiba 278-8510, Japan

<sup>c</sup>Institute of Laser Engineering (ILE), Osaka University,

Yamadaoka 2-6, Suita, Osaka 565-0871, Japan

<sup>d</sup>Research Center for Nuclear Physics (RCNP), Osaka University,

Mihogaoka 10-1, Ibaraki, Osaka 567-0047, Japan

---

<sup>1</sup>e-mail: sumi@numazu-ct.ac.jp

<sup>2</sup>e-mail: suzuki@ph.noda.tus.ac.jp

<sup>3</sup>Present address: Science and Engineering, Waseda University, e-mail: shoichi@heap.phys.waseda.ac.jp

<sup>4</sup>e-mail: toki@rcnp.osaka-u.ac.jp

## Abstract

We study characteristics of the relativistic equation of state (EOS) for collapse-driven supernovae, which is derived by relativistic nuclear many body theory. Recently the relativistic EOS table has become available as a new complete set of physical EOS for numerical simulations of supernova explosion. We examine this EOS table by using general relativistic hydrodynamics of the gravitational collapse and bounce of supernova cores. In order to study dense matter in dynamical situation, we perform simplified calculations of core collapse and bounce by following adiabatic collapse with the fixed electron fraction for a series of progenitor models. This is intended to give us “approximate models” of prompt explosion. We investigate the profiles of thermodynamical quantities and the compositions during collapse and bounce. We also perform the calculations with the Lattimer-Swesty EOS to compare the properties of dense matter. As a measure of the stiffness of the EOS, we examine the explosion energy of the prompt explosion with electron capture totally suppressed. We study the derivative of the thermodynamical quantities obtained by the relativistic EOS to discuss the convective condition in neutron-rich environment, which may be important in the delayed explosion.

# 1 Introduction

Clarifying the mechanism of core-collapse supernova explosion is fascinating. It is a challenging problem which demands extensive research efforts in physics and astrophysics. Towards the final answer, one has to conduct sophisticated numerical simulations treating all ingredients of microphysics and macrophysics. Recently, numerical simulations solving hydrodynamics together with the Boltzmann equation for the neutrino transfer have become available in spherical symmetry [1, 2, 3, 4, 5, 6]. In these simulations, the basic equations of hydrodynamics and neutrino transfer have been solved directly together with the careful implementation of microphysics. This recent progress, removing one of uncertainties due to approximate neutrino transfer, has shed light again on the importance of the microphysics such as neutrino interactions and properties of dense matter.

An important microphysics ingredient for supernova simulations is the equation of state (EOS) of dense matter. It determines the stellar structure, the hydrodynamics and the reaction rates through the determination of pressure, entropy and chemical compositions. Although study of dense matter for supernova research apparently has a long history, there are only a few studies to cover the whole range of density, electron fraction and temperature in supernova environment. Because one has to simulate the whole phenomena starting from collapsing iron cores to cooling neutron stars, it is necessary to provide thermodynamical quantities in a wide range of density, composition and temperature in a usable and complete form for numerical simulations. Such efforts to provide the EOS have been done so far by a limited number of groups. The EOS formulated in terms of nuclear parameters by Baron, Cooperstein and Kahana [7] has been used to study the influence of the EOS on the explosion. Hillebrandt and Wolff [8] have taken the Skyrme Hartree-Fock approach to provide the data table of EOS for supernova simulations. This EOS table has been used in some simulations [8, 9, 10], but is not currently used. Lattimer and Swesty [11] have utilized the compressible liquid-drop model to provide the EOS as a numerical routine for supernova simulations. This EOS has been used in many simulations of supernova explosion these years. However, it has been difficult to assess the dependence of the supernova phenomena on the EOS since available EOS's based on different nuclear models are limited (See, however, [12, 13, 14, 15]).

Recently, a new complete EOS for supernova simulations has become available [16, 17]. The relativistic mean field (RMF) theory with a Thomas-Fermi approach has been applied to the derivation of the supernova EOS. The RMF theory has been successful to reproduce the saturation properties, masses and radii of nuclei, and proton-nucleus scattering data [18]. The effective interaction used in the RMF theory is checked by the recent experimental data of unstable nuclei in neutron-rich environment close to astrophysical situations.

We stress that the RMF theory is based on the relativistic Brückner-Hartree-Fock (RBHF) theory [19]. The RBHF theory, which is a microscopic and relativistic many body theory, has been shown to be successful to reproduce the saturation of nuclear matter starting from the nucleon-nucleon interactions determined by the scattering experiments. This is in good contrast with non-relativistic many body frameworks which can account for the saturation only with the introduction of extra three-body interactions. The effective lagrangian of the RMF theory has been extended to take account of the behavior of the RBHF theory [20]. It is also noteworthy that relativistic frameworks automatically satisfy the causality, which is the condition that the sound velocity should not exceed the light velocity, while the causality is often violated in non-relativistic frameworks.

Having a new set of EOS table, numerical simulations of hydrodynamics with neutrino transfer are awaited to investigate the influence of the relativistic EOS on the supernova dynamics as well as supernova neutrinos. Before we proceed to such elaborate numerical simulations, which require large computational efforts, we would like to examine the properties of the relativistic EOS in dynamical situation during supernova explosion which may not be apparent in a common practice of calculations of neutron star structure. It will also be helpful to provide the basic information on the behavior of relativistic EOS during collapse and bounce for forthcoming detailed simulations. For this purpose, we perform hydrodynamical calculations of adiabatic collapse with the relativistic EOS table dropping off the treatment of neutrino transfer. We adopt presupernova models by Woosley-Weaver [21] and Nomoto et al. [22] as realistic initial models. We fix the electron fraction at the initial value, which maximizes the shock energy at bounce, as working models of explosion. With these “trial models”, we examine the properties of dense matter such as compositions obtained from our EOS during core collapse

and bounce. We evaluate the energy of shock at breakout as one of measures of the EOS for a series of presupernova models. For comparison, we perform the hydrodynamical calculations with the Lattimer-Swesty EOS and explore the difference of the properties of dense matter and the shock energy.

In addition to getting the information mentioned above, we would like to test whether the relativistic EOS table works well in numerical simulations during core collapse and explosion. This is because some EOS tables so far have been causing troubles in numerical simulations due to lack or inconsistency of data. The relativistic EOS table has been calculated in a wide regime of environment (density, proton fraction and temperature) to provide all necessary quantities of dense matter, which are tabulated for numerical simulations [17] of various astrophysical phenomena such as supernovae and neutron star mergers.

This paper is arranged as follows. In section 2, after a brief introduction of collapse-driven supernova explosions, we explain our hydrodynamical calculations which are used for the study of the relativistic EOS. In section 3, we present our numerical results. We first show the initial profiles of presupernova core derived with the relativistic EOS table (section 3.1). In section 3.2, we display the profiles of thermodynamical quantities from the relativistic EOS during collapse and bounce. We compare the results with the case using the Lattimer-Swesty EOS. In section 4, we also discuss the effect of the relativistic EOS on the Ledoux criterion of convection. Summary will be given in section 5.

## 2 Hydrodynamical simulation

### 2.1 Treatment of core-collapse and explosion

The collapse-driven supernova explosion originates from massive stars with  $M \geq 10M_{\odot}$  (for reviews, see [23, 24, 25], for example). At the end of the thermonuclear stellar evolutions, the iron core is formed at the center of a presupernova star. This iron core becomes gravitationally unstable and starts collapsing due to the photo-dissociation and electron captures, which reduce the pressure to support the core. The gravitational collapse proceeds homologously in the inner part of the iron core and supersonically in the outer part of the iron core. When the central

density exceeds the nuclear matter density, the inner core bounces back due to a hard core component of nuclear force. Due to this bounce, a shock wave is formed and it propagates outward. The shock wave goes through the outer core region, consuming its energy to dissociate irons into nucleons and to push back the falling material against the gravitational attraction.

If the shock wave reaches the surface of the iron core without stalling on the way, it blows off the mantle outside the iron core to cause a supernova explosion. This simple scenario of hydrodynamical explosion is called “prompt explosion”. If the shock wave stalls inside the outer core region, some extra mechanism is necessary to revive the stalled shock. For example, the neutrino heating behind the shock might save the failed shock wave and give a successful supernova explosion in a relatively long time scale around 100 msec. This type of supernova mechanism is called “delayed explosion”.

Although prompt explosion is a simple scenario, it is generally believed that the explosion does not occur in this way for a major fraction of progenitors (see recent studies in [4, 5, 6]). In the past, Baron et al. have found that the prompt explosion occurs for the combination of soft EOS’s and general relativistic hydrodynamics [7]. However, later studies by Myra and Bludman [26] have shown that those explosions obtained in an approximate leakage scheme do not occur in a better treatment of neutrino transport (multigroup flux-limited diffusion approximation) with an appropriate treatment of neutrino interactions such as neutrino-electron scattering. Further systematic investigations by Bruenn and Swesty et al. [13, 14, 15] have confirmed that no prompt explosion occurs except for extreme range of parameters of EOS and presupernova stars. Because of the difficulty of prompt explosion, especially for massive stars such as SN1987A, the delayed mechanism is believed to be the cause of the explosion. However, detailed processes to revive the stalled shock have been under debates [25].

The EOS plays essential roles in supernova dynamics both in direct and indirect manners. A softer EOS gives more compact cores at bounce with larger binding energy and provides larger energy to shock wave. The dependence of supernova explosion on the softness of EOS has been studied by changing incompressibility of nuclear matter [7, 14, 15] (See also [27] in a different context). Smaller incompressibility is indeed found to be preferable.

The composition of dense matter is also another important factor of explosion. The abun-

dances of proton, neutron, alpha particle and nucleus determine the reaction rates of electron captures, neutrino scatterings and others. The species of nucleus in dense matter is essential for evaluation of the electron capture rate on nuclei. When the electron captures on nuclei are suppressed in the high density regime, the free proton fraction is important to determine the electron capture rate on protons (see, however, [28] on the importance of electron captures on nuclei). Those electron capture rates control the neutrino emissivity during the collapse, resultant trapped lepton fraction and the size of inner core. A larger inner core leads to a larger initial shock energy and a smaller outer core through which the shock wave must propagate. Therefore, it is preferable for shock propagations if the EOS provides the composition which suppresses electron captures. For the determination of composition, the description of nuclear interaction for nuclei and matter is essential. As for the free proton fraction, it is closely related to the symmetry energy. The influence of the free proton fraction on supernova explosion has been studied [13, 15]. It has been found that larger symmetry energies provide smaller free proton fractions, which lead to a larger electron fraction.

In the current study, we investigate the properties of the relativistic EOS using the collapse and bounce of the supernova cores. Since the new EOS table is derived in the relativistic many body framework unlike the previous EOS sets for supernova simulations, we would like to know the basic properties of the new EOS in a dynamical context. Since the current EOS table is based on the data of unstable nuclei and the symmetry energy part of nuclear interactions is better constrained, the composition of dense matter may be different from those in the previous EOS sets. Since we employ simplified adiabatic collapse with no neutrino transfer, we do not intend to discuss the supernova mechanism itself. Instead, the current study will provide the basic information of the relativistic EOS table in the physical situations close to the realistic supernova explosion and will serve as a guide to proceed to more sophisticated numerical simulations.

We adopt the implicit numerical code for the general relativistic and spherically symmetric hydrodynamics [29]. The implicit time differencing is advantageous to carry the hydrodynamical calculations for a long time. The code uses a Lagrangian baryon mass coordinate (baryon mass enclosed within a certain radius) as a radial coordinate. We refer to the article by Yamada [29]

for details of the numerical treatment of hydrodynamics. This numerical code is specifically designed for the study of supernova explosion to treat both the hydrodynamics and the neutrino transfer. The Boltzmann solver of neutrino transfer is recently implemented in the numerical code [2]. Detailed simulations of gravitational core collapse based on this fully implicit and general relativistic code with neutrino transfer will be presented elsewhere.

## 2.2 Equation of state of dense matter

We adopt the table of the relativistic EOS, which is recently derived for supernova simulations [16, 17] in the relativistic nuclear many body framework. Based on the relativistic Brückner-Hartree-Fock theory, which is successful to reproduce the nuclear matter saturation, the relativistic mean field (RMF) theory is constructed to describe nuclear matter and nuclei [20]. The same RMF framework has been applied to the systematic study of about 2000 nuclei, including deformed ones, up to the drip line in the nuclear chart and the nuclear data such as masses and radii are successfully reproduced [30]. Having thus being checked by the data of stable and unstable nuclei, the RMF framework has been used to study the properties of dense matter in supernovae [31]. The RMF framework with the parameter set TM1, which was determined as the best one to reproduce the properties of finite nuclei [20], provides the uniform nuclear matter with the incompressibility of 281 MeV and the symmetry energy of 36.9 MeV at the saturation density. We remark that the behavior of nuclear matter at high density in the RMF framework is similar to the one in the relativistic Brückner-Hartree-Fock theory due to the inclusion of the non-linear terms in the RMF lagrangian. The maximum neutron star mass calculated for the cold neutron star matter in the RMF with TM1 is  $2.2 M_{\odot}$ . The RMF framework has been extended with the Thomas-Fermi approximation to describe not only the homogenous but also inhomogeneous matter in supernovae, which contains neutrons, protons, alpha particles and heavy nuclei as a representative species. The properties of dense matter (energy, pressure, entropy, chemical potential and so on) at various densities, proton fractions and temperatures are calculated to construct the numerical data table for simulations. The table covers the wide range of density ( $10^{5.1} \sim 10^{15.4}$  g/cm<sup>3</sup>), electron fraction (0.0  $\sim$  0.56), and temperature (0  $\sim$  100 MeV), which is required for supernova simulations. The relativistic EOS



table is available upon request to one of the authors, K. Sumiyoshi. The electron/positron and photon contributions as non-interacting particles are added to the nuclear contribution of the EOS. The relativistic EOS table has been applied to numerical simulations of r-process in the neutrino-driven winds [32] and in supernova explosions [33]. A proto-type of the EOS table has been used in the numerical simulations of the proto-neutron star cooling [34].

For comparison, we adopt also the EOS by Lattimer and Swesty [11], which has been used for recent supernova simulations. The EOS is based on the compressible liquid drop model for nuclei together with dripped nucleons [35]. The bulk energy of nuclear matter is expressed in terms of density, proton fraction and temperature with nuclear parameters. The values of nuclear parameters are chosen to be the ones suggested from nuclear mass formulae and other theoretical studies mostly with the Skyrme  $I'$  force. Among various parameters, the symmetry energy is set to be 29.3 MeV, which is smaller than the value in the relativistic EOS. As for the incompressibility, there are three choices with different values of 180, 220, 375 MeV. We use, for comparison, the EOS with 180 MeV, which has been often used for supernova studies.

## 2.3 Initial models

We adopt the presupernova models of massive stars provided by Woosley (WW95) [21, 36] and by Nomoto (N97) [22, 37] (see also [38]). From WW95, we have used 11, 12, 13, 15, 18 and 20  $M_{\odot}$  models among the models ranging from  $11M_{\odot}$  to  $40M_{\odot}$ . From N97, we have used the models with Helium cores of 3.3, 4, 5 and 6  $M_{\odot}$ , which correspond to the progenitor mass of 13, 15, 18 and 20  $M_{\odot}$ , respectively. In Table 1, we list the models we have used for the calculations. We utilize the central core part which covers the Fe core and the outer layer with the density down to about  $10^6$  g/cm<sup>3</sup>. The masses of the calculated central core and the Fe core are listed also in Table 1. We take density, electron fraction, temperature and radius as a function of baryon mass coordinate from the original data and derive other quantities using the relativistic EOS table. The number of the baryon mass grid points is 100. The grid size decreases linearly from the center to the surface to provide enough grid points around the surface. As for the outer boundary condition, we fixed density, internal energy, entropy and electron fraction of the most outer grid point at the original values in the initial model. The original configuration

of the central core of the presupernova models is already marginally unstable to gravitational collapse. When we start the numerical calculation with the constructed initial configuration, the inner core starts collapsing immediately. We have checked that, if we increase slightly the electron fraction in the original models, the core remains stable and does not start collapsing. Therefore, the profile of electron fraction in the models has just marginal values to trigger the gravitational collapse.

## 3 Numerical results

### 3.1 Initial Composition

Before we proceed to the results of hydrodynamics, we discuss the composition of the central core derived with the relativistic EOS table. The composition just prior to the collapse is interesting since it affects the trapped lepton fraction through weak interactions. The trapped lepton fraction in turn determines the size of the inner core and the available explosion energy. The species of nuclei in the central core are important to evaluate the electron capture rates on nuclei in the hot and dense matter. After the electron capture on nuclei is blocked due to the nuclear shell effects, the electron capture on free protons becomes important. Therefore, the mass fraction of free protons is also important quantity to determine the evolution of electron (lepton) fraction during the collapse stage [23, 24].

Figure 1 displays the mass fraction of particles (upper panel), the proton, neutron and mass numbers of nuclei (lower panel) as a function of baryon mass coordinate in the central core of  $15M_{\odot}$  model of WW95. The values with the relativistic EOS and the Lattimer-Swesty EOS [11] are shown by thick and thin lines, respectively. The quantities of the Lattimer-Swesty EOS are obtained by giving the same profiles of density, temperature and electron fraction (See Fig. 4 for the initial profile of density).

In the upper panel, the initial profile of electron fraction is also shown. The central value of electron fraction in the initial model is 0.42. It can be seen that the mass fractions are substantially different between the relativistic EOS and the Lattimer-Swesty EOS. The mass fractions of alpha particle and neutron in the relativistic EOS are larger than those in the

Lattimer-Swesty EOS. The free proton fraction is about one order of magnitude smaller than the numbers obtained with the Lattimer-Swesty EOS. Having a smaller fraction of free proton is favorable for the explosion since the electron capture is largely reduced, leading to a stronger prompt-shock [13].

The reduction of free proton fraction comes from an effect of the large symmetry energy. A larger symmetry energy provides a larger difference between chemical potentials of protons and neutrons. A lower chemical potential for protons leads to a smaller free proton fraction and a higher chemical potential for neutrons gives a larger free neutron fraction. Note that the symmetry energy of the relativistic EOS (36.9 MeV) is larger than that of the Lattimer-Swesty EOS (29.3 MeV). The value of the symmetry energy is constrained mainly by nuclear masses, but there is still an allowable range. Systematic measurements of the radii of neutron-rich nuclei may further constrain the size of the symmetry energy since the thickness of neutron skins is sensitive to the symmetry energy. We stress that the symmetry energy of the relativistic EOS has been checked by the nuclear structure calculations of the radii of neutron-rich nuclei in the RMF framework [20, 39] together with the recent experimental data of neutron skins [40, 41].

It has been known that the relativistic many body frameworks provide a larger effect of the symmetry energy on nuclei and uniform nuclear matter than the non-relativistic many body frameworks [42]. The relativistic many body frameworks provide stronger density dependence of the symmetry energy. Accordingly, the proton fraction in the cold neutron star matter in the relativistic many body frameworks is larger than that in the non-relativistic frameworks [43]. A large proton fraction can lead to the rapid cooling of neutron stars due to the direct URCA process [44]. At the same time, the thickness of neutron skins of neutron-rich nuclei is enhanced in the relativistic frameworks. It has been shown that the systematics of neutron skins of isotopes and the EOS of asymmetric matter are related to each other and the behavior of asymmetric matter can be probed by systematic measurements of unstable nuclei [45]. A precise measurement of neutron radius of  $^{208}\text{Pb}$  in future would provide more information on the EOS of asymmetric matter [46, 47]. It is interesting to see if these differences of the nuclear properties coming from the new relativistic frameworks have influence on the supernova explosion through the change of compositions and reaction rates.

It is remarkable that heavy nuclei beyond  $A=60$  appear in a wide region of the core. It is also interesting to see that the neutron number exceeds 40 in the central region, where electron capture might be suppressed according to the shell blocking [48, 49] (see, however, [28]). Compared with the results in the Lattimer-Swesty EOS, the species of nuclei is about 10% heavier. The slightly larger value of binding energy of nuclear matter in the relativistic EOS table ( $B=16.3$  MeV) than in the Lattimer-Swesty EOS ( $B=16.0$  MeV), and/or the different treatments of nuclear surface, neutron skin and translational energy affect the determination of species, which should be studied further carefully. These findings of heavier nuclei may suggest that the detailed study of electron capture rates in  $A=60$  region and beyond is important for the outcome of the core collapse. In recent shell-model calculations [50, 51] of weak-interaction rates for nuclei in the mass range  $A=45-65$  in the stellar environment, electron capture rates are significantly smaller than the standard set of Fuller, Fowler and Newman [52, 53, 54, 55]. Calculations of presupernova evolution of massive stars with improved rates for weak interactions [56] provide larger electron fractions, leading to a possible increase of explosion energy. This trend of suppression of electron capture on nuclei might be a key toward successful explosions and it strengthens the motivation to study core collapse in detail by the improved EOS and weak interactions.

One has to be cautious, however, that there is a negative feedback in the deleptonization during collapse. If the electron fraction is large in the initial stage, the free proton fraction becomes large and electron captures on free protons drives back the electron fraction small. Resulting trapping lepton fractions turn out similar even from the different electron fractions in progenitors [57]. This is because the free proton fraction depends steeply on the electron fraction. For example, the free proton fraction becomes smaller by a factor of 10 if we decrease the electron fraction by  $\Delta Y_e = 0.03$  from the value ( $Y_e = 0.42$ ) at the center of initial model. We have looked into the case of the Lattimer-Swesty EOS and have found that the dependence of the free proton fraction on the electron fraction is similar in this region. To get the same value with the Lattimer-Swesty EOS for the free proton fraction, a larger value by  $\Delta Y_e \sim 0.02$  can be possible in the relativistic EOS. If the electron captures would proceed up to a certain value of the free proton fraction, the resulting lepton fraction might be larger by about 0.02,

which might lead to a slightly larger inner core, in the relativistic EOS. Whether this difference of the free proton fraction influences the core collapse remains to be seen in more detailed calculations.

We note here that the current comparison is made by adopting the temperature profiles from the presupernova models instead of the entropy profiles. One has to be careful about the choice of thermodynamical inputs (temperature or entropy) to discuss the composition of matter since the composition is sensitive to temperature. Extensive comparisons with the Lattimer-Swesty EOS during the core collapse and bounce are currently being made and will be published elsewhere.

### 3.2 Profiles during core collapse and bounce

Figures 2 and 3 demonstrate successful and unsuccessful explosions in hydrodynamical calculations starting from the initial configurations of the 15 and 20  $M_{\odot}$  presupernova models of WW95. In the cases of 11, 12 and 15  $M_{\odot}$  models, a shock wave launched at the core bounce goes through the outer core, leading to a successful prompt explosion. On the other hand, in the cases of 13, 18 and 20  $M_{\odot}$  models, a shock wave stalls after the bounce due to photodissociation and infalling material. We list up the size of iron core in Table 1. It is natural to see that the success of prompt explosion is clearly correlated with the size of iron core. The size of iron core is small ( $1.32M_{\odot}$ ) in all the successful cases, whereas it exceeds  $1.4M_{\odot}$  in the unsuccessful cases. Interestingly, the 13  $M_{\odot}$  model has an iron core of  $1.41 M_{\odot}$ , being different from neighboring 11 and 15  $M_{\odot}$  models and does not show a prompt explosion. In the cases of N97 models, the explosion is successful for 13, 15 and 18  $M_{\odot}$ . The size of iron core is again small ( $1.18, 1.28$  and  $1.36 M_{\odot}$  for 13, 15 and 18  $M_{\odot}$  models, respectively) in these cases [22]. The case of 20  $M_{\odot}$  model does not show a prompt explosion. The size of iron core in this case is  $1.40 M_{\odot}$ , which suggests that the threshold is around  $1.4M_{\odot}$ .

Explosion energy amounts to 1.7 foe (foe =  $10^{51}$  erg) for 11 and 12  $M_{\odot}$  models and 1.5 foe for 15  $M_{\odot}$  model of WW95, whereas 1.8, 1.7 and 1.7 foe for 13, 15 and 18  $M_{\odot}$  models of N97, respectively. Here we define that the explosion energy is the energy of ejecta (gravitational mass minus baryon mass of ejecta) in the general relativistic formulation (see Appendix and [29]).

We list up the explosion energy and the remnant mass for the cases of successful explosion in Table 1. These results confirm the correspondence between the iron core mass (not progenitor mass) and explosion energy. It has been argued that a smaller iron core mass results in a larger explosion energy since the amount of dissociation of iron nuclei becomes smaller for the similar size of unshocked cores [58] (see also [24]). We note here again that the electron fraction is fixed at the initial value, which maximizes the shock energy at bounce, in order to obtain working models of explosion. The explosion energy evaluated here is the maximum value attained with the relativistic EOS table and should be regarded as one of measures of the stiffness of EOS.

In more realistic simulations with the neutrino transfer, the shock energy is lost also by the cooling due to neutrino emissions and the pressure by falling material in addition to the dissociation of iron nuclei. Whether the stalled shock wave revives or not depends probably on the neutrino heating mechanism and the explosion energy may depend more on how the delayed explosion occurs.

It is instructive to display profiles of quantities during the core collapse and bounce. We show, in Figs. 4–6, the density, velocity and entropy as a function of baryon mass coordinate for various times. We choose the case of  $15 M_{\odot}$  model of WW95 as a representative model and concentrate on the profiles of quantities calculated with this model for further discussions.

In Fig. 4, we display the density profiles when the central densities reach  $10^{11}$ ,  $10^{12}$ ,  $10^{13}$ ,  $10^{14}$  g/cm<sup>3</sup> during the collapse (1–4) as well as the density profiles around and after the bounce (5–14). The initial density profile is also shown (0). The central density becomes high ( $2.1 \times 10^{14}$  g/cm<sup>3</sup>) at the stage (5) and a density jump propagates outward. The peak central density is  $4.0 \times 10^{14}$  g/cm<sup>3</sup> at the stage (10), which corresponds to the bounce at the time 322 msec after the onset of the collapse. The central density decreases slightly to  $3.3 \times 10^{14}$  g/cm<sup>3</sup> at the stage (14) at the time 12 msec after the bounce.

In the velocity profiles in Fig. 5, the development of shock structure is apparent. At the stages (1–4), the inner homologous collapse and the outer free fall can be seen. A pressure wave starts at the center (5) and develops at the stages (6–9). It becomes a shock wave at the border of the inner core at the stage (10). The positive velocity peak starts growing and the outward shock wave proceeds toward the surface of the iron core (11–14).

The profiles of entropy per baryon are shown in Fig. 6. Because it is an adiabatic collapse, the central entropy per baryon stays around  $1k_B$  (1–5). The entropy is raised as the shock wave propagates and reaches above a few  $k_B$  at the bounce (10). The shocked envelope with high entropy ( $\sim 10 k_B$ ) is formed at (11–14). During these sequences, the central temperature increases to  $\sim 5$  MeV during the collapse (1–5) and becomes as high as 10 MeV at the bounce (6–10). The temperature peak is formed at the outer core due to the shock passage and the temperature exceeds 20 MeV at the maximum (11–14).

We describe here shortly a numerical simulation with the Lattimer-Swesty EOS of which results are also shown for comparison. We run a hydrodynamical calculation starting from the same initial configuration of the  $15 M_\odot$  model of WW95. A prompt explosion occurs with the explosion energy of 1.9 foe, which is larger than the case of the relativistic EOS. The peak central density is found to be  $5.3 \times 10^{14}$  g/cm<sup>3</sup>, which is also higher. Using the result of hydrodynamics with the Lattimer-Swesty EOS, we compare the compositions at the times having the same central densities during the collapse and at the times having the same position of the shock wave after the bounce.

The compositions during collapse and bounce are shown in Figs. 7–10. The notations are the same as in Fig. 1. The mass fractions during collapse are shown as a function of baryon mass coordinate at the times (1) and (2) (central densities:  $10^{11}$ ,  $10^{12}$  g/cm<sup>3</sup>) in Fig. 7, at the times (3) and (4) ( $10^{13}$ ,  $10^{14}$  g/cm<sup>3</sup>) in Fig. 8. During collapse (1–2) in Fig. 7 the mass fraction of nuclei decreases slightly and alpha particles, protons and neutrons become more abundant. The difference between the Lattimer-Swesty EOS and the relativistic EOS, which is seen in Fig. 1, is present in early stages of collapse. The difference becomes less drastic and the compositions become similar in later stages (3–4) in Fig. 8. The mass fraction of alpha particle remains larger than that in the Lattimer-Swesty EOS. Alpha particles are abundant in the outer part of the core ( $M_B > 1.0M_\odot$ ) during core collapse and bounce. The mass fractions around bounce (7) and (9) are shown in Fig. 9. Neutrons and protons are dominant at the central region after bounce because of high density and temperature. This region grows due to dissociation of nuclei as the shock wave proceeds outward. The difference between the relativistic EOS and the Lattimer-Swesty EOS in the central region is small. The appearance

of nuclei at  $M_B \sim 0.3M_\odot$  for the Lattimer-Swesty EOS at the stage (7) may be attributed to their treatment of the phase boundary.

The mass and proton numbers during collapse (1–3) and around bounce (4–9) are shown as a function of baryon mass coordinate in Fig. 10. The nuclei become heavier and more neutron-rich as the central density increases. This tendency is stronger in the relativistic EOS than in the Lattimer-Swesty EOS. We note that the neutron skin of nuclei is taken into account in the relativistic EOS but not in the Lattimer-Swesty EOS which may cause different mass number and neutron-richness. After bounce, huge nuclei appear in the relativistic EOS at the density around  $10^{14}$  g/cm<sup>3</sup>. This is in contrast to the case of the Lattimer-Swesty EOS, which gives nuclei up to the mass number of 200. This is because of the different treatment of nuclear shape change and bubble phase just below the nuclear matter density. In the relativistic EOS table, those effects are not included like Lattimer et al. [35] (LLPR) whereas the Lattimer-Swesty EOS takes them into account and finds smaller nuclear masses than LLPR. The zig-zag behavior of mass number and proton number around  $M_B \sim 1.0M_\odot$  is due to the fact that the density-temperature trajectories go around the phase boundary between nuclei and gas, where the mass fractions change rapidly.

The adiabatic indices at around the bounce stages (7) and (9) are shown as a function of baryon mass coordinate in Fig. 11. The case of the Lattimer-Swesty EOS is shown by thin lines for comparison. The adiabatic index in the relativistic EOS is larger than that of the Lattimer-Swesty EOS in the central region where the density exceeds  $10^{14}$  g/cm<sup>3</sup>. In the outer region, they are similar to each other except for some fluctuations due to the phase transition we mentioned above. This difference in the central region indicates that the relativistic EOS is stiffer at these densities than the Lattimer-Swesty EOS in terms of the adiabatic index. Since the central density is not far beyond the nuclear matter density, the behavior is mostly determined by the incompressibility. The value of the incompressibility of the relativistic EOS (K=281 MeV) is larger than the value (K=180 MeV) we adopted for the Lattimer-Swesty EOS.

The stiffness can be discussed in terms of the shock energy described above and the size of the inner core. We have examined whether the explosion energy can be explained in terms of the initial shock energy due to the bounce of the inner core and the dissociation of iron nuclei



due to the shock passage in the outer core [24]. As a reference, we list the size of inner core in Table 1. In Fig. 5, one can clearly see the structure with an unshocked inner core and an infalling outer core. Here, we define the inner core as the region inside the edge of positive velocity in the profile when the velocity turns from negative to positive in the central region (see the bounce stage 10). For both WW95 and N97 models, the inner core mass is about  $0.9 M_{\odot}$  independent of the progenitor mass. The inner cores and remnant masses in the case of the Lattimer-Swesty EOS are also similar.

We plot in Fig. 12 the profiles of the enclosed energy (i.e.  $(m_g - m_b)$  in Appendix) in the case of  $15 M_{\odot}$  model of WW95. The upper and lower panels correspond to the stages (10) and (14), respectively. The upper panel (a) corresponds to the bounce when the shock wave with positive velocity just starts to show up and the lower panel (b) shows the situation after the shock wave have passed through the iron core.

While the enclosed energy of the inner core becomes large at first due to the compression and amounts to  $1.1 \times 10^{52}$  erg at  $M_B = 0.87 M_{\odot}$  in Fig. 12a, it decreases, in Fig. 12b, to  $5.7 \times 10^{51}$  erg as it approaches the final hydrostatic configuration due to decompression (see also Fig. 4). The difference of these energies is the initial shock energy of  $5.6 \times 10^{51}$  erg. The shock loses its energy due to the dissociation of irons when it passes through the outer iron core. The dissociation of irons between  $M_B = 0.87 M_{\odot}$  (the inner core mass,  $M_{inner}$ ) and  $M_B = 1.14 M_{\odot}$  (the remnant mass,  $M_{remn}$ ) requires the energy of  $4.3 \times 10^{51}$  erg. Due to this energy loss, the shock energy is reduced to  $1.3 \times 10^{51}$  erg, which corresponds to the final explosion energy transferred to the ejected material. In realistic simulations with electron captures, the inner core mass will be smaller than the present case in which the electron capture and the neutrino interaction are artificially suppressed. If the inner core mass were smaller by  $\sim 0.1 M_{\odot}$  than the present case, the shock wave would lose more energy ( $\sim 1.6 \times 10^{51}$  erg, corresponding to  $\sim 0.1 M_{\odot}$ ) during the propagation and, therefore, the prompt explosion should become more difficult.

We remark that the numerical data table of the relativistic EOS works properly in the hydrodynamical calculations without troubles such as overflows of range due to the lack of data or the inconsistency of thermodynamical properties. We have monitored the total energy during

the numerical simulation and have checked that the total energy after the hydrodynamical calculation agrees with the initial total energy with enough numerical accuracy of  $\sim 10^{-6}$ .

## 4 Outlook on further effects

It has been discussed that the delayed explosion through the revival of shock due to neutrino-heating might be a general mechanism of supernova explosion [25]. The detailed processes in micro- and macro-physics can play significant roles to realize the explosion of this type. One has to treat carefully all interactions, which change lepton fractions in dense matter and lead to heating and cooling. We stress that the EOS of dense matter provides the information such as compositions and chemical potentials and is essential to determine those reaction rates. For example, the effective mass of nucleon is tabulated in the table. It might affect the neutrino opacity substantially [59]. Detailed studies by the numerical simulations with neutrino transfer using the relativistic EOS table are under way [60].

We have to remark also that the current study is done under the spherical symmetry. Deviations from the spherical symmetry such as matter mixing have been suggested by the observations of light curve and line profiles of SN1987A. Multi-dimensional effects such as convection can play an important role in the explosion mechanism [23, 25, 61]. However, where, when and how long hydrodynamical instabilities occur in the central region of a supernova and how it contributes to the explosion mechanism are a matter of long debates. On one hand, the convection has been shown to be essential for the successful delayed explosion through neutron fingers [62]. On the other hand, it has been claimed that the neutron finger convection is unlikely to occur [63]. Other recent studies have demonstrated that the whole proto-neutron star just born may be convective, which will be favorable for the explosion [64] (see, however, [65]). The diffusive processes in the convection have been also discussed recently in detail [66].

In the current study, we have aimed to see the properties of the relativistic EOS as a basis for further studies. Multi-dimensional simulations of supernova explosion with the relativistic EOS table is of great interest given the present results. In order to assess the influence of the relativistic EOS on multi-dimensional hydrodynamics, we focus on the convective instability inside the neutrinosphere and investigate the condition derived by the relativistic EOS.

The negative gradients of the entropy and/or the lepton fraction are often seen in a number of numerical simulations (see [34] for example) and can lead to the convective overturn. The convection can raise the hot and lepton-rich matter toward the neutrinosphere and enhance the neutrino luminosities to heat the region just behind the stalled shock. This extra heating can be crucial to revive the stalled shock leading to a successful delayed explosion.

Here, we discuss a role of EOS in the Ledoux criterion, the condition that the convection occurs without diffusive processes by the gradient of entropy and lepton fraction. This means that the EOS is also essential to judge whether convection occurs or not through the distributions of these quantities. The Ledoux criterion is expressed by,

$$\left(\frac{\partial\rho}{\partial Y_l}\right)_{P,S} \cdot \left(\frac{dY_l}{dr}\right) + \left(\frac{\partial\rho}{\partial S}\right)_{P,Y_l} \cdot \left(\frac{dS}{dr}\right) \geq 0, \quad (1)$$

where  $\rho$ ,  $Y_l$ ,  $S$  are density, lepton fraction and entropy per baryon, respectively. The derivatives of density with respect to lepton fraction,

$$\left(\frac{\partial\rho}{\partial Y_l}\right)_{P,S}, \quad (2)$$

and with respect to entropy,

$$\left(\frac{\partial\rho}{\partial S}\right)_{P,Y_l}, \quad (3)$$

are usually assumed to be negative. Hence the negative gradient of entropy and/or lepton fraction inside stars leads to the convection. However, the derivative of density with respect to lepton fraction can change its sign in a certain environment [67]. Note that the derivative of density with respect to entropy per baryon is always negative.

We investigate this point with the relativistic EOS. For this purpose, we consider the dense matter under thermal and beta equilibrium among neutrons, protons, electrons, positrons, three flavor (anti-)neutrinos and photons. Basic properties of this supernova matter have been reported in [31]. Figure 13 displays the sign of derivative and the borders of the sign change for the cases of the entropy per baryon  $S = 1, 2$  and  $4$  by solid, dashed and dash-dotted lines, respectively. It is remarkable that the derivative is positive in the region with high density and low lepton fraction. This is in accord with the previous results by Lattimer and Mazurek [67] and other recent works [68, 69]. We note, however, that the positive sign region tends to be much wider than the previous results at high densities due to the effect of the larger

symmetry energy. We stress here an important role of the nuclear symmetry energy, which is well constrained by the experiments of unstable nuclei, and is properly taken into account in the relativistic EOS.

The sign change happens because the nuclear interaction contributes to the pressure on top of the lepton contribution. The contribution of symmetry energy dominates in the neutron-rich (low lepton fraction) environment. An increase in lepton fraction not only leads to the increase in lepton pressure, but also leads to the decrease of baryonic pressure due to nuclear interactions. Therefore, the density must increase to keep the pressure constant in this positive sign regime. The convection is then stabilized by the negative gradient of lepton fraction. On the contrary, the positive gradient of lepton fraction can lead to convection if the entropy per baryon is constant. Therefore, an extra attention should be paid to the convective region itself in multi-dimensional simulations with the relativistic EOS.

## 5 Summary

We have studied the properties of the relativistic EOS during the core collapse and bounce in supernovae. The relativistic EOS table is newly derived based on the relativistic many body theory checked by the experimental data of unstable nuclei and is available for astrophysical simulations. To examine the properties of dense matter given by the relativistic EOS in dynamical situations of supernova explosion, we have utilized the general relativistic hydrodynamical calculations of gravitational collapse of iron cores.

In order to provide the basic information of the relativistic EOS before we proceed to detailed numerical simulations, we have followed the adiabatic collapse with the fixed electron fraction without neutrino transfer and have obtained model explosions. Because of the high electron fraction, which is fixed at the initial value, the inner core mass is large and the hydrodynamical explosion is obtained. We have examined the thermodynamical quantities and compositions of dense matter during collapse and bounce in these model explosions. We have compared the compositions with those in the Lattimer-Swesty EOS by performing the corresponding adiabatic collapse calculation. We have evaluated the explosion energy for a series of progenitor models as one of measures of the stiffness of EOS. We have also discussed that the relativistic EOS

might have an influence on the condition of convection. We have seen that the numerical data table of the relativistic EOS works quite successfully in the numerical simulations.

We have found that the initial composition in presupernova cores is fairly different from that in the Lattimer-Swesty EOS. The difference of composition persists during early stages of collapse and becomes less significant at and after bounce. The mass fraction of protons at the early stages is much smaller than that in the Lattimer-Swesty EOS because of the large symmetry energy in the relativistic nuclear many body theory. The mass fraction of alpha particles is larger during the whole stage. The species of nuclei is found to be heavier and more neutron-rich during collapse and the mass number turns out to be quite large after bounce. Compositional differences may lead to changes in electron capture rates and neutrino interaction rates and might influence the dynamics of supernova explosion.

These differences of compositions should be examined further in numerical simulations of hydrodynamics with neutrino transfer by switching the two sets of EOS. Detailed simulations including the neutrino transfer with this new relativistic EOS table are called for to examine the role of the EOS in the delicate mechanism of supernova explosion. Such efforts of numerical simulations are currently being made [60].

## Acknowledgment

We would like to express special thanks to Hong Shen for her devoted achievement of the relativistic EOS table and to H. Ono for his great efforts on the tabulation of the Lattimer-Swesty EOS. We would like to thank Stan Woosley and Ken'ichi Nomoto for providing us with their numerical data of presupernova models. K. S. is grateful to M. Terasawa, G. Mathews, T. Kajino and I. Tanihata for fruitful collaborations on r-process nucleosynthesis in supernova explosions. K. S. also thanks S. Wanajo, A. Onishi, K. Oyamatsu and Thomas Janka for stimulating discussions. The numerical simulations have been performed on the supercomputers at RIKEN and KEK (KEK Supercomputer Projects No.01-75 and No.02-87). This work is partially supported by the Grants-in-Aid for the Center-of-Excellence (COE) Research of the ministry of Education, Science, Sports and Culture of Japan to RESCEU (No.07CE2002). This work is also supported in part by Japan Society for Promotion of Science, and by the Grant-in

Aid for Scientific Research (12047230, 12740138, 13740165, 14039210, 14740166, 15740160) of the Ministry of Education, Science, Sports and Culture of Japan.

## Appendix

We summarize here the definitions of gravitational mass, baryon mass and explosion energy in general relativity. The notation mostly follows those in the reference [29]. We take  $c = G = 1$  in the following equations.

The baryon mass elements in spherical symmetry is given by

$$dm_b = \frac{\rho_b}{\Gamma} 4\pi r^2 dr, \quad (\text{A-1})$$

and the baryon mass coordinate is defined accordingly as

$$m_b = \int_0^r \frac{\rho_b}{\Gamma} 4\pi r'^2 dr'. \quad (\text{A-2})$$

Here,  $\rho_b$  is the baryon mass density and  $\Gamma$  is the relativistic gamma factor defined by,

$$\Gamma^2 = 1 + U^2 - \frac{2m_g}{r}. \quad (\text{A-3})$$

$U$  is the radial fluid velocity and  $m_g$  is the gravitational mass defined below. The gravitational mass,  $dm_g$ , of the baryon mass elements,  $dm_b$ , is given by

$$dm_g = \rho_b (1 + \varepsilon) 4\pi r^2 dr, \quad (\text{A-4})$$

$$= \Gamma(1 + \varepsilon) dm_b, \quad (\text{A-5})$$

where  $\varepsilon$  is the specific internal energy density. The gravitational mass is then given by

$$m_g = \int_0^{m_b} \frac{dm_g}{dm_b} dm_b, \quad (\text{A-6})$$

$$= \int_0^r \rho_b (1 + \varepsilon) 4\pi r'^2 dr'. \quad (\text{A-7})$$

The gravitational mass of ejecta is evaluated by

$$M_g^{ejecta} = \int_{M_{remn}}^{M_{calc}} \frac{dm_g}{dm_b} dm_b, \quad (\text{A-8})$$

where the range of integral in baryon mass coordinate is from the remnant mass,  $M_{remn}$ , to the total baryon mass covered in the calculation,  $M_{calc}$ . The remnant mass is defined at the

position in the baryon mass coordinate where the minimum of the enclosed energy ( $m_g - m_b$ ) occurs (see Fig. 12, for example). The explosion energy is calculated as

$$E_{exp} = M_g^{ejecta} - M_b^{ejecta}, \quad (\text{A-9})$$

where the baryon mass of ejecta is

$$M_b^{ejecta} = M_{calc} - M_{remn}. \quad (\text{A-10})$$

# References

- [1] A. Mezzacappa and S.W. Bruenn, *Astrophys. J.* 405 (1993) 669.
- [2] S. Yamada, H.-Th. Janka and H. Suzuki, *A&A* 344 (1999) 533.
- [3] A. Burrows, T. Young, P. Pinto, R. Eastman and T.A. Thompson, *Astrophys. J.* 539 (2000) 865.
- [4] M. Rampp and H.-T. Janka, *Astrophys. J.* 539 (2000) L33.
- [5] A. Mezzacappa, M. Liebendörfer, O.E.B. Messer, W.R. Hix, F.-K. Thielemann and S.W. Bruenn, *Phys. Rev. Lett.* 86 (2001) 1935.
- [6] M. Liebendörfer, A. Mezzacappa, F.-K. Thielemann, O.E.B. Messer, W.R. Hix and S.W. Bruenn, *Phys. Rev. D* 63 (2001) 103004.
- [7] E. Baron, J. Cooperstein and S. Kahana, *Phys. Rev. Lett.* 55 (1985) 126.
- [8] W. Hillebrandt and R.G. Wolff, *Nucleosynthesis-Challenges and New Developments*, edited by W.D. Arnett and J.M. Truran, (Univ. of Chicago, Chicago, 1985), p.131.
- [9] H. Suzuki, *Neutrino burst from supernova explosion and proto neutron star cooling*, Ph.D. thesis, University of Tokyo (1990).
- [10] H. Suzuki, in *Proceedings of the International Symposium on Neutrino Astrophysics: Frontiers of Neutrino Astrophysics*, edited by Y. Suzuki and K. Nakamura, (Universal Academy Press Inc., Tokyo, 1993), No. 5 in *Frontiers Science Series*, p.219.
- [11] J.M. Lattimer and F.D. Swesty, *Nucl. Phys. A* 535 (1991) 331.
- [12] S.W. Bruenn, *Astrophys. J. Suppl.* 62 (1986) 331.
- [13] S.W. Bruenn, *Astrophys. J.* 340 (1989) 955.
- [14] S.W. Bruenn, *Astrophys. J.* 341 (1989) 385.
- [15] F.D. Swesty, J.M. Lattimer and E.S. Myra, *Astrophys. J.* 425 (1994) 195.



- [16] H. Shen, H. Toki, K. Oyamatsu and K. Sumiyoshi, Nucl. Phys. A637 (1998) 435.
- [17] H. Shen, H. Toki, K. Oyamatsu and K. Sumiyoshi, Prog. Theor. Phys. 100 (1998) 1013.
- [18] B.D. Serot and J.D. Walecka, in Advances in Nuclear Physics, edited by J.W. Negele and E. Vogt (Plenum Press, New York, 1986), Vol. 16, p.1.
- [19] R. Brockmann and R. Machleidt, Phys. Rev. C42 (1990) 1965.
- [20] Y. Sugahara and H. Toki, Nucl. Phys. A579 (1994) 557.
- [21] S.E. Woosley and T. Weaver, Astrophys. J. Suppl. 101 (1995) 181.
- [22] K. Nomoto, M. Hashimoto, T. Tsujimoto, F.-K. Thielemann, N. Kishimoto, Y. Kubo and N. Nakasato, Nucl. Phys. A616 (1997) 79c.
- [23] H.A. Bethe, Rev. Mod. Phys. 62 (1990) 801.
- [24] H. Suzuki, Physics and Astrophysics of Neutrinos, edited by M. Fukugita and A. Suzuki, (Springer-Verlag, Tokyo, 1994), p.763.
- [25] H.-Th. Janka, K. Kifonidis and M. Rampp, Proc. of Workshop on Physics of Neutron Star Interiors (ECT\*, Trento, 2000), edited by D. Blaschke, N.K. Glendenning, A.D. Sedrakian, Springer, Lect. Notes Phys. 578 (2001) 333.
- [26] E.S. Myra and S.A. Bludman, Astrophys. J. 340 (1989) 384.
- [27] M. Takahara and K. Sato, Astrophys. J. 335 (1988) 301.
- [28] K. Langanke, G. Martinez-Pinedo, J.M. Sampaio, D.J. Dean, W.R. Hix, O.E.B. Messer, A. Mezzacappa, M. Liebendoerfer, H.-Th. Janka and M. Rampp, Phys. Rev. Lett. 90 (2003) 241102.
- [29] S. Yamada, Astrophys. J. 475 (1997) 720.
- [30] D. Hirata, K. Sumiyoshi, I. Tanihata, Y. Sugahara, T. Tachibana and H. Toki, Nucl. Phys. A616 (1997) 438c.

- [31] K. Sumiyoshi, H. Kuwabara and H. Toki, Nucl. Phys. A581 (1995) 725.
- [32] K. Sumiyoshi, H. Suzuki, K. Otsuki, M. Terasawa and S. Yamada, Pub. Astron. Soc. Japan 52 (2000) 601.
- [33] K. Sumiyoshi, M. Terasawa, G.J. Mathews, T. Kajino, S. Yamada, and H. Suzuki, Astrophys. J. 562 (2001) 880.
- [34] K. Sumiyoshi, H. Suzuki and H. Toki, A&A 303 (1995) 475.
- [35] J.M. Lattimer, C.J. Pethick, D.G. Ravenhall and D.Q. Lamb, Nucl. Phys. A432 (1985) 646.
- [36] S.E. Woosley, private communication (1999).
- [37] K. Nomoto, private communication (2000).
- [38] K. Nomoto and M. Hashimoto, Phys. Rep. 163 (1988) 13.
- [39] Y. Sugahara, K. Sumiyoshi, H. Toki, A. Ozawa and I. Tanihata, Prog. Theor. Phys. 96 (1996) 1165.
- [40] T. Suzuki *et al.*, Phys. Rev. Lett. 75 (1995) 3241.
- [41] A. Ozawa *et al.*, Nucl. Phys. A691 (2001) 599.
- [42] K. Sumiyoshi, D. Hirata, H. Toki and H. Sagawa, Nucl. Phys. A552 (1993) 437.
- [43] K. Sumiyoshi, K. Oyamatsu and H. Toki, Nucl. Phys. A595 (1995) 327.
- [44] J.M. Lattimer, C.J. Pethick, M. Prakash and P. Haensel, Phys. Rev. Lett. 66 (1991) 2701.
- [45] K. Oyamatsu, I. Tanihata, Y. Sugahara, K. Sumiyoshi and H. Toki, Nucl. Phys. A634 (1998) 3.
- [46] B.A. Brown, Phys. Rev. Lett. 85 (2000) 5296.
- [47] C.J. Horowitz and J. Piekarewicz, Phys. Rev. C66 (2002) 055803.
- [48] G.M. Fuller, Astrophys. J. 252 (1982) 741.

- [49] S.W. Bruenn, *Astrophys. J. Suppl.* 58 (1985) 771.
- [50] E. Caurier, K. Langanke, G. Martinez-Pinedo and F. Nowacki, *Nucl. Phys.* A653 (1999) 439.
- [51] K. Langanke and G. Martinez-Pinedo, *Nucl. Phys.* A673 (2000) 481.
- [52] G.M. Fuller, W.A. Fowler and M.J. Newman, *Astrophys. J. Suppl.* 42 (1980) 447.
- [53] G.M. Fuller, W.A. Fowler and M.J. Newman, *Astrophys. J.* 252 (1982) 715.
- [54] G.M. Fuller, W.A. Fowler and M.J. Newman, *Astrophys. J. Suppl.* 48 (1982) 279.
- [55] G.M. Fuller, W.A. Fowler and M.J. Newman, *Astrophys. J.* 293 (1985) 1.
- [56] A. Heger, S.E. Woosley, G. Martinez-Pinedo and K. Langanke, *Astrophys. J.* 560 (2001) 307.
- [57] M. Liebendörfer, O.E.B. Messer, A. Mezzacappa, W.R. Hix, F.-K. Thielemann and K. Langanke, *Proc. of the 11th Workshop on Nuclear Astrophysics (Ringberg Castle, Munich, 2002)*, edited by W. Hillebrandt and E. Müller, astro-ph/0203260.
- [58] D.W. Arnett, *Astrophys. J.* 263 (1982) L55.
- [59] S. Yamada and H. Toki, *Phys. Rev.* C61 (2000) 015803.
- [60] K. Sumiyoshi, S. Yamada, H. Suzuki and H. Toki, in preparation (2003).
- [61] R. Epstein, *MNRAS* 188 (1979) 305.
- [62] J.R. Wilson and R.W. Mayle, *Phys. Rep.* 227 (1993) 97.
- [63] S.W. Bruenn, A. Mezzacappa and T. Dineva, *Phys. Rep.* 256 (1995) 69.
- [64] W. Keil, H.-T. Janka and E. Müller, *Astrophys. J.* 473 (1996) L111.
- [65] R. Buras, M. Rampp, H.-Th. Janka and K. Kifonidis, *Phys. Rev. Lett.* 90 (2003) 241101.
- [66] J.A. Miralles, J.A. Pons and V.A. Urpin, *Astrophys. J.* 543 (2000) 1001.

- [67] J.M. Lattimer and T.J. Mazurek, *Astrophys. J.* 246 (1981) 955.
- [68] S.W. Bruenn and T. Dineva, *Astrophys. J.* 458 (1996) L71.
- [69] A. Mezzacappa, A.C. Calder, S.W. Bruenn, J.M. Blondin, M.W. Guidry, M.R. Strayer and A.S. Umar, *Astrophys. J.* 493 (1998) 848.

# Table caption

**Table 1** The list of models with different progenitor masses ( $M_{proj}$ ) of WW95 (a) and N97 (b). The sizes (in baryon mass) of iron core ( $M_{Fe}$ ), core covered in calculation ( $M_{calc}$ ) and inner core ( $M_{inner}$ ) obtained in simulations are listed. The remnant mass ( $M_{remn}$ ) and explosion energy ( $E_{exp}$ ) are listed for successful cases.

**Table 1a**

Model	$M_{proj} [M_{\odot}]$	$M_{Fe} [M_{\odot}]$	$M_{calc} [M_{\odot}]$	$M_{inner} [M_{\odot}]$	$M_{remn} [M_{\odot}]$	$E_{exp} [10^{51} \text{ erg}]$
S11A	11	1.32	1.42	0.87	1.15	1.7
S12A	12	1.32	1.36	0.86	1.08	1.7
S13A	13	1.41	1.62	0.87	—	—
S15A	15	1.32	1.56	0.87	1.14	1.5
S18A	18	1.46	1.84	0.89	—	—
S20A	20	1.74	2.20	0.88	—	—
S15A-LS	15	1.32	1.56	0.87	1.15	1.9

**Table 1b**

Model	$M_{proj} [M_{\odot}]$	$M_{Fe} [M_{\odot}]$	$M_{calc} [M_{\odot}]$	$M_{inner} [M_{\odot}]$	$M_{remn} [M_{\odot}]$	$E_{exp} [10^{51} \text{ erg}]$
3.3	13	1.18	1.38	0.83	1.06	1.8
4	15	1.28	1.41	0.83	1.08	1.7
5	18	1.36	1.62	0.85	1.13	1.7
6	20	1.40	1.67	0.84	—	—

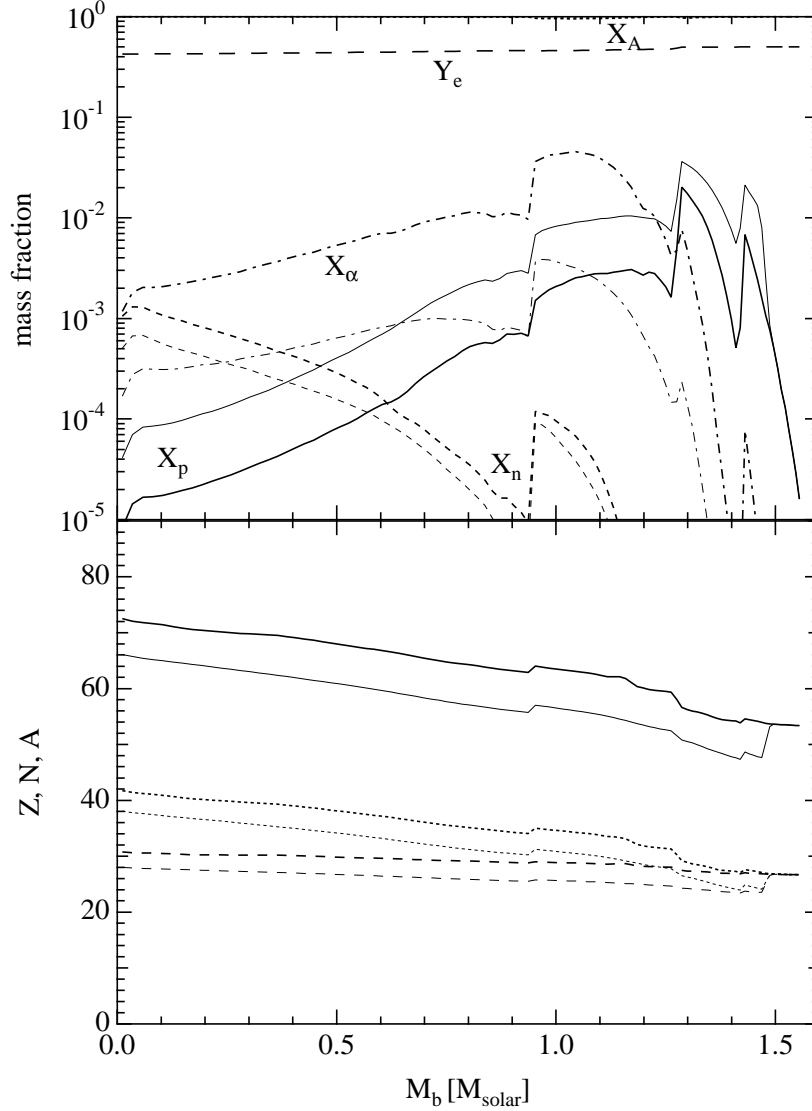


Figure 1: The mass fraction of particles (upper panel), the mass, neutron and proton numbers of nuclei (lower panel) in the core of  $15 M_\odot$  model (WW95) are shown as a function of baryon mass coordinate. The results obtained with the relativistic EOS are shown by thick lines and the Lattimer-Swesty EOS by thin lines. Solid, dashed, dotted and dot-dashed lines in the upper panel show mass fractions of protons, neutrons, nuclei and alpha particles, respectively. Long dashed line in the upper panel displays the initial electron fraction. Solid, dotted and dashed lines in the lower panel show the mass, neutron and proton numbers of nuclei, respectively.

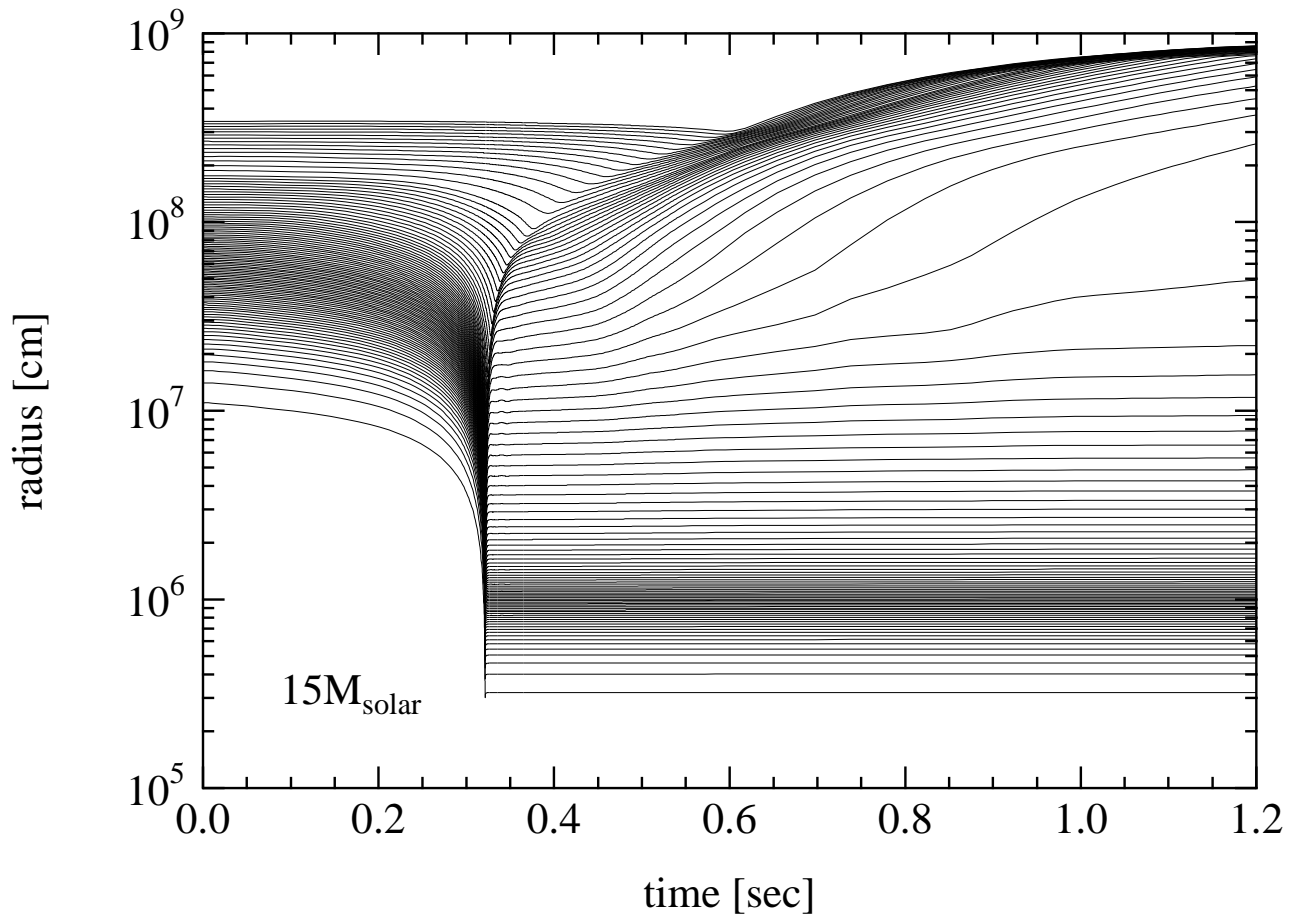


Figure 2: The trajectories of mass mesh in radius are displayed as a function of time in hydrodynamical calculation of  $15 M_{\odot}$  models of WW95.

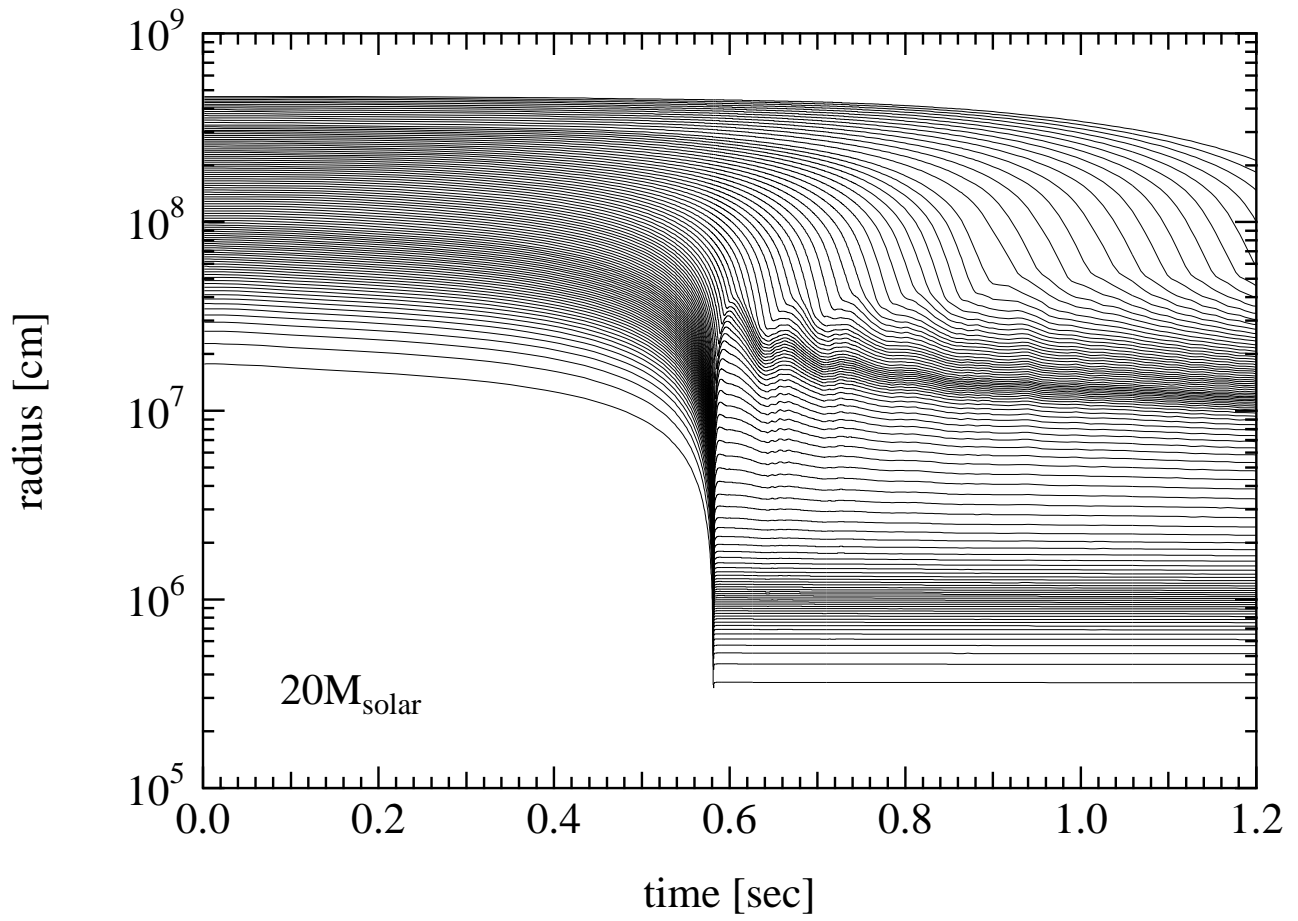


Figure 3: The trajectories of mass mesh in radius are displayed as a function of time in hydrodynamical calculation of  $20 M_{\odot}$  models of WW95.



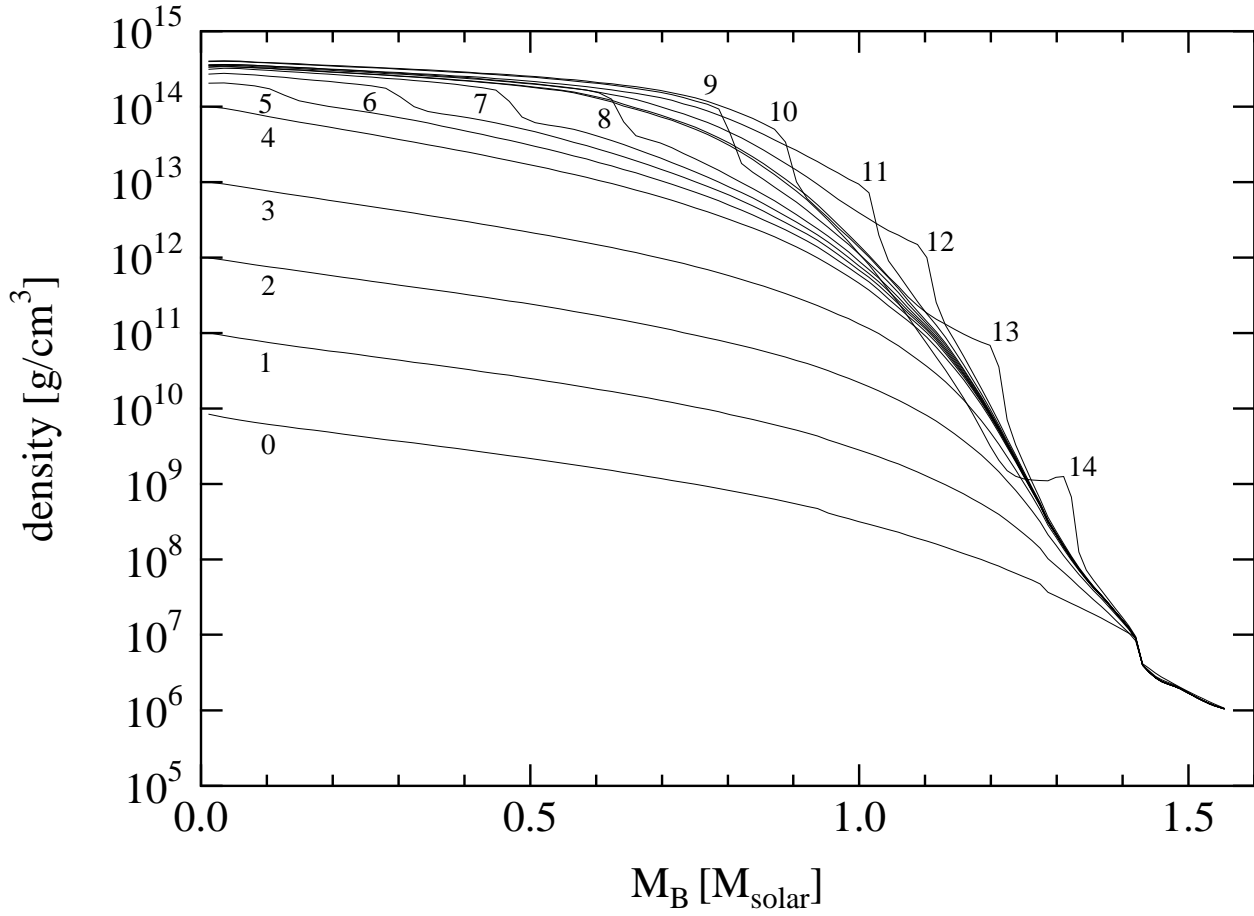


Figure 4: The density profiles at selected times are shown as a function of baryon mass coordinate for the case of  $15 M_{\odot}$  model of WW95. Indices denote the time sequence as explained in the text.

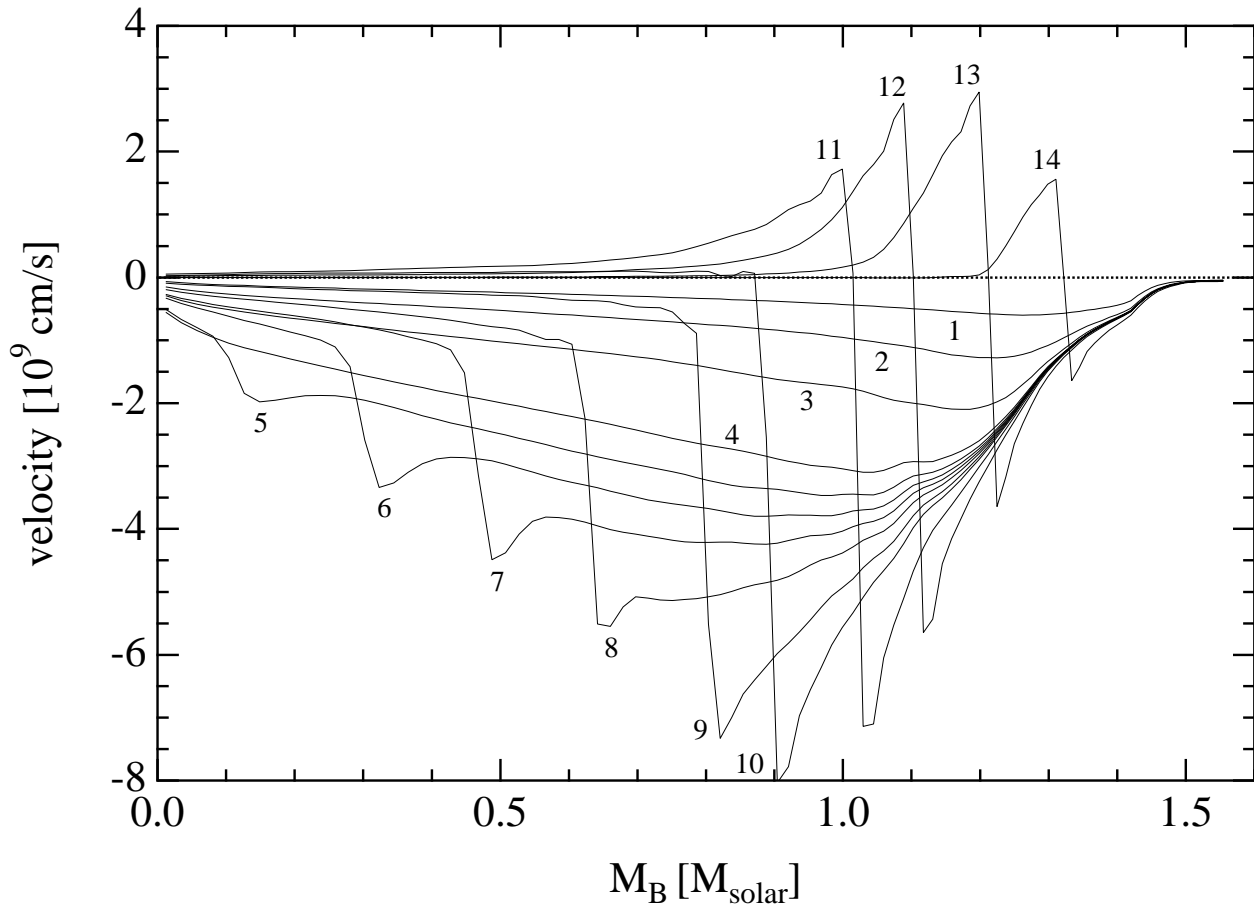


Figure 5: The velocity profiles at selected times are shown as a function of baryon mass coordinate.

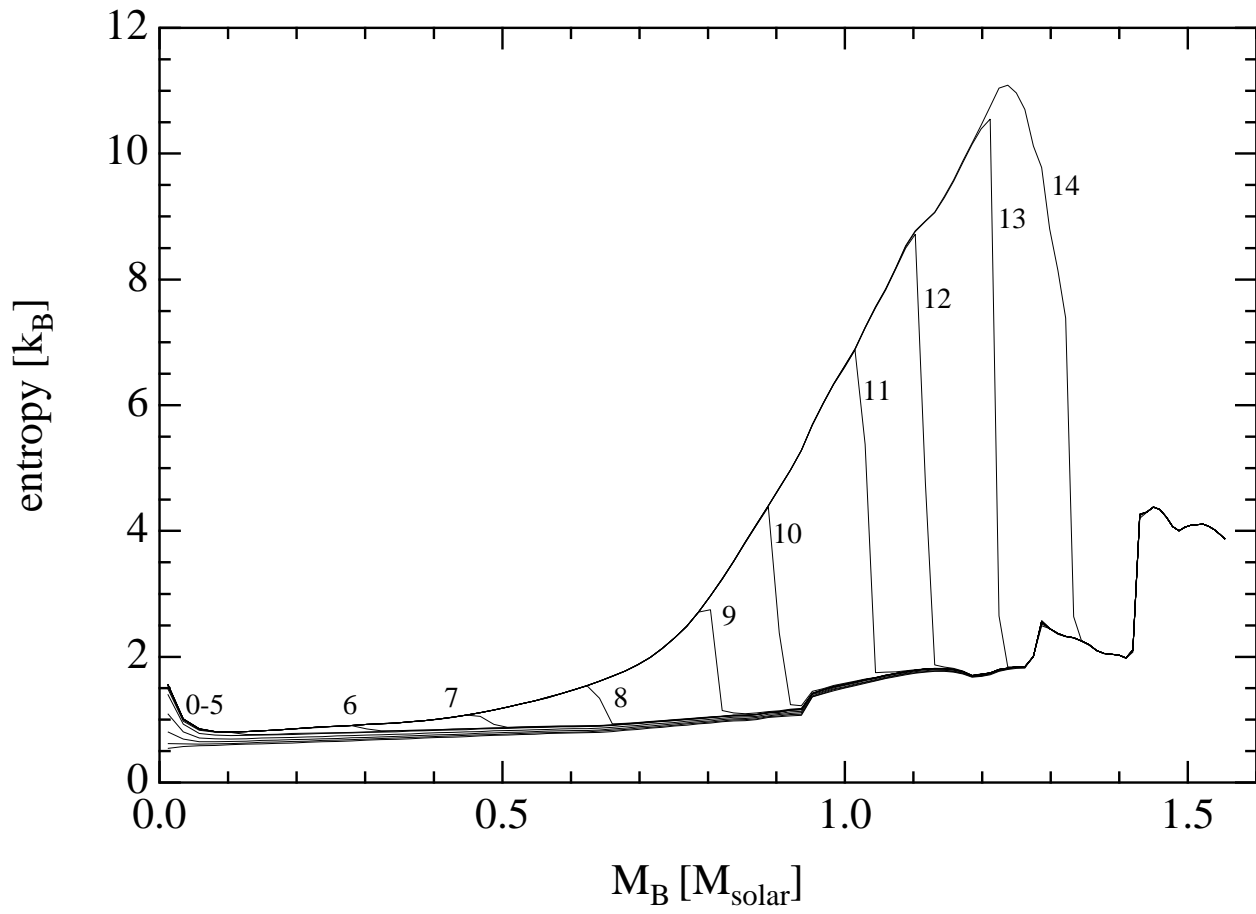


Figure 6: The entropy per baryon profiles at selected times are shown as a function of baryon mass coordinate.

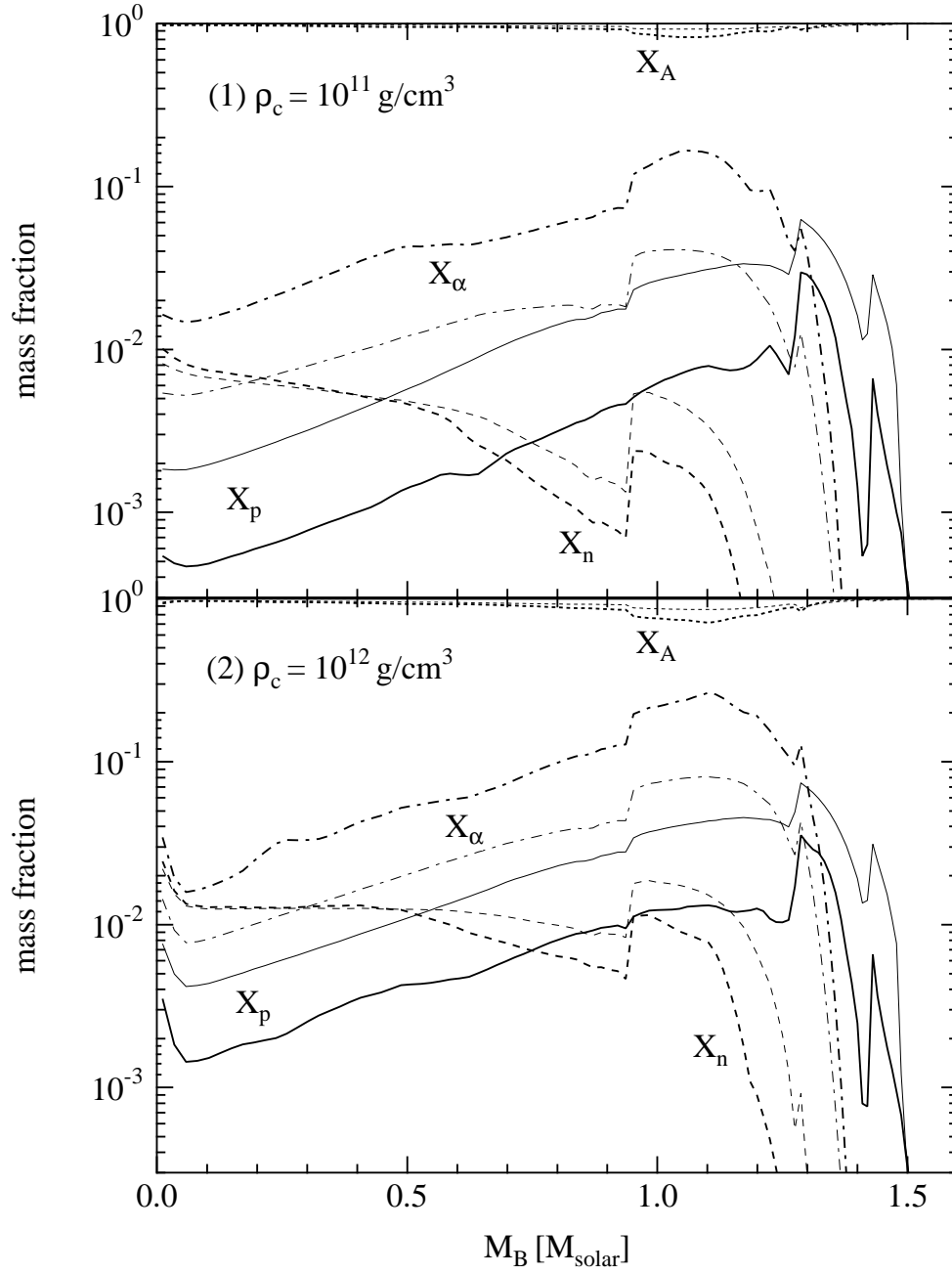


Figure 7: The mass fractions of protons, neutrons, nuclei and alpha particles are shown as a function of baryon mass coordinate at the collapse stages (1, 2) for the case of  $15 M_{\odot}$  model of WW95. The notations are the same as in Fig. 1.

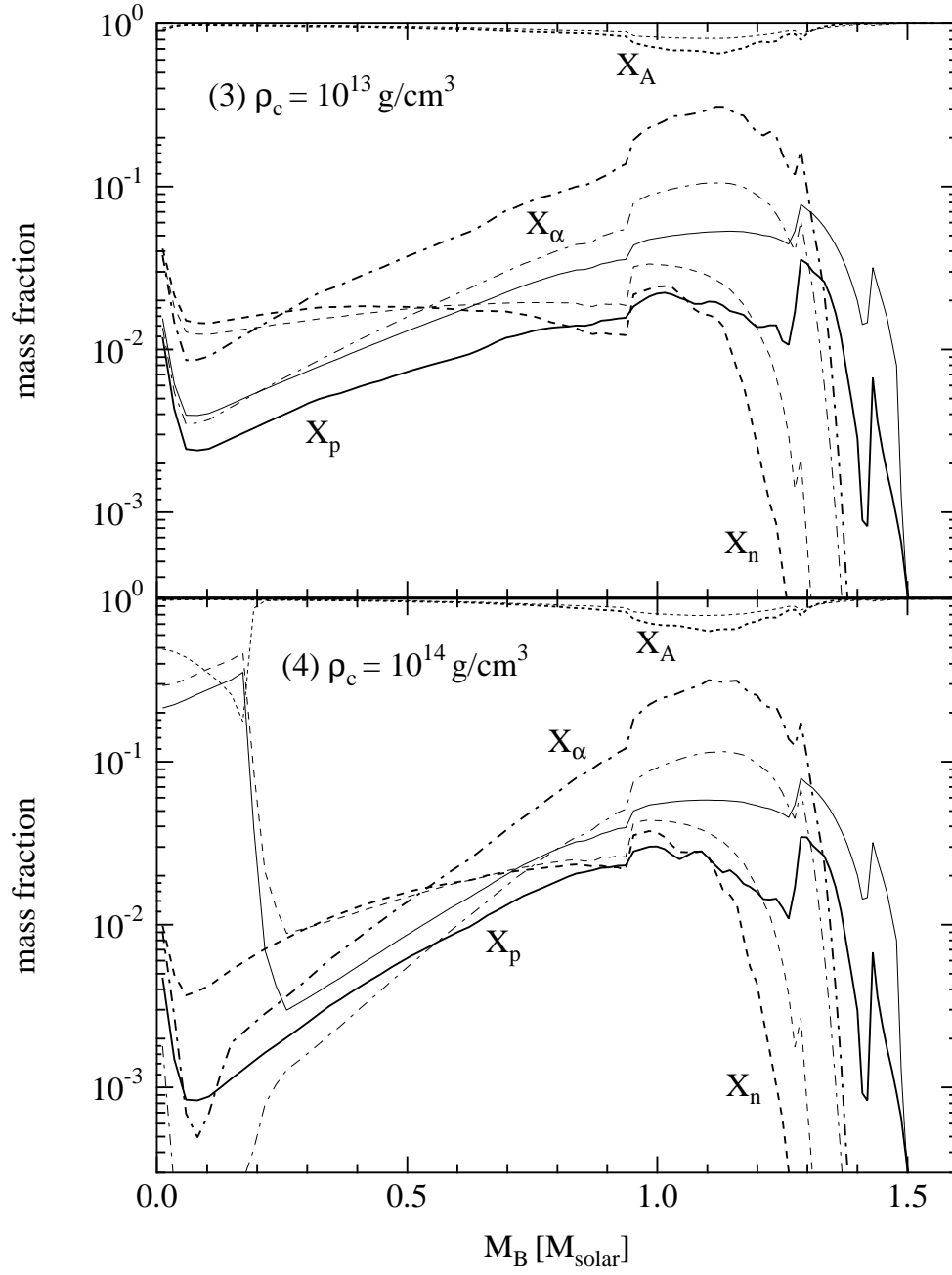


Figure 8: The mass fractions of protons, neutrons, nuclei and alpha particles are shown as a function of baryon mass coordinate at the collapse stages (3, 4). The notations are the same as in Fig. 1.

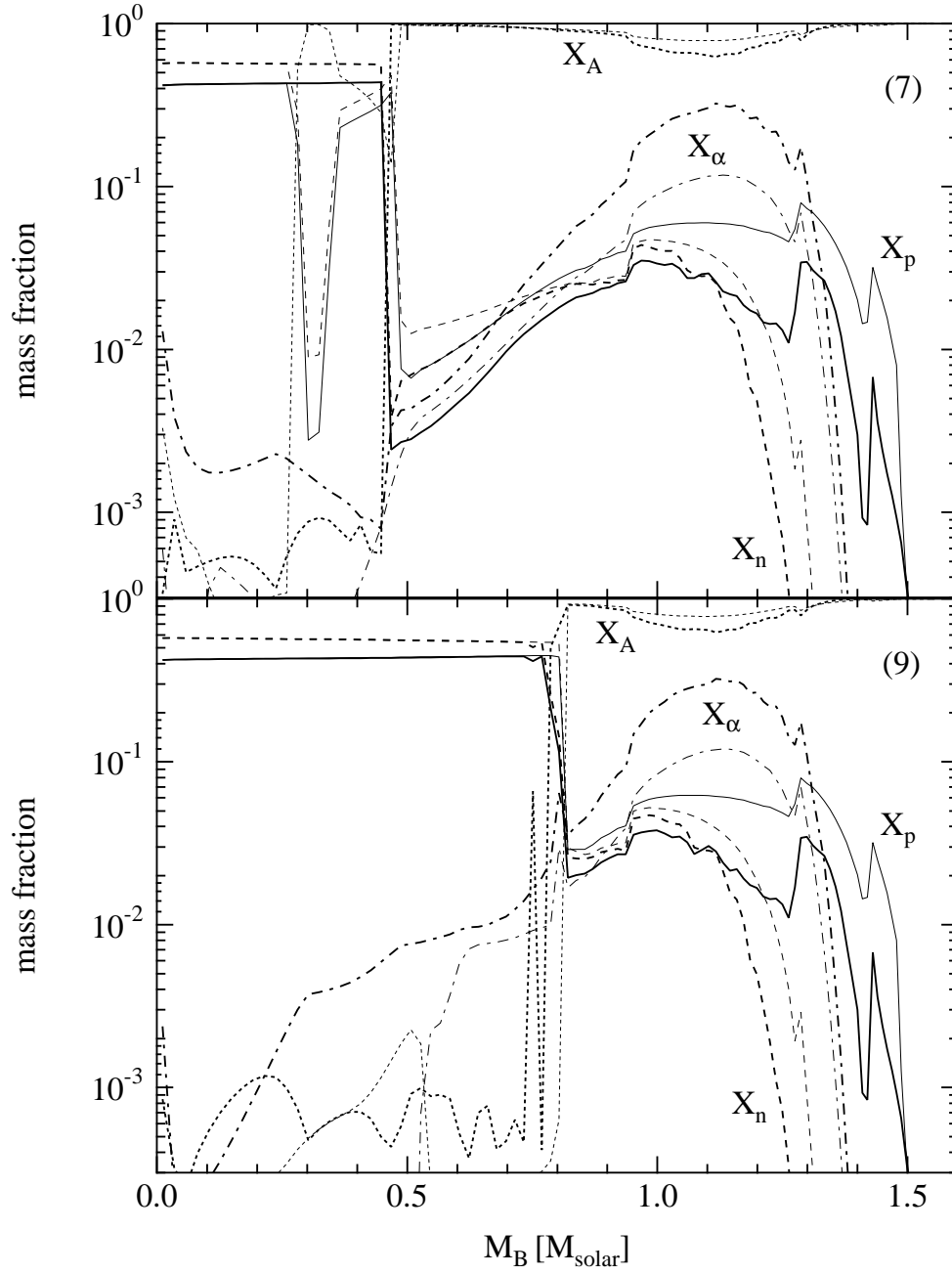


Figure 9: The mass fractions of protons, neutrons, nuclei and alpha particles are shown as a function of baryon mass coordinate at around the bounce stages (7, 9). The notations are the same as in Fig. 1.

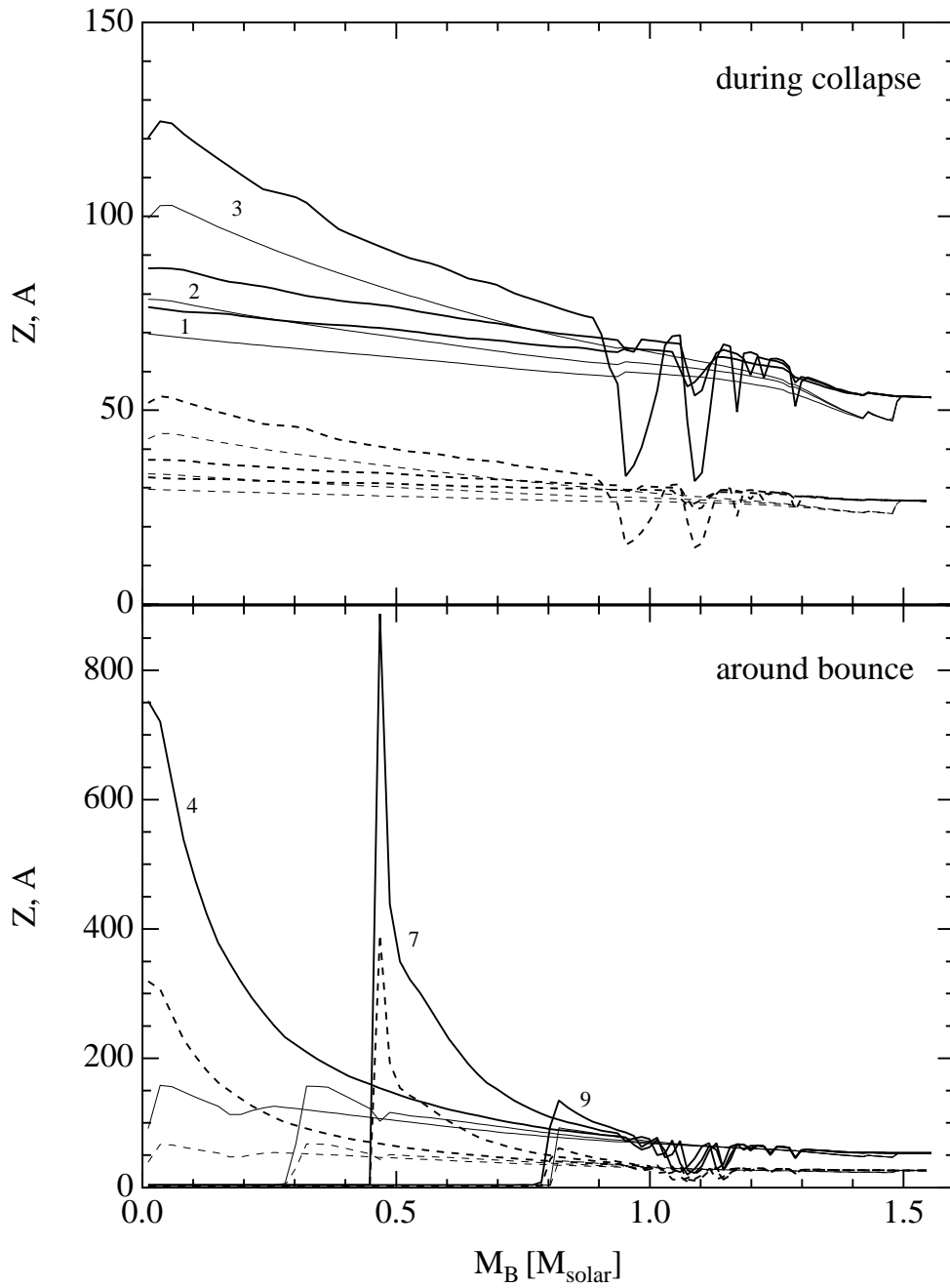


Figure 10: The mass and proton number of nuclei are shown as a function of baryon mass coordinate at the collapse stages (1,2,3) and around the bounce stages (4,7,9). The notations are the same as in Fig. 1.

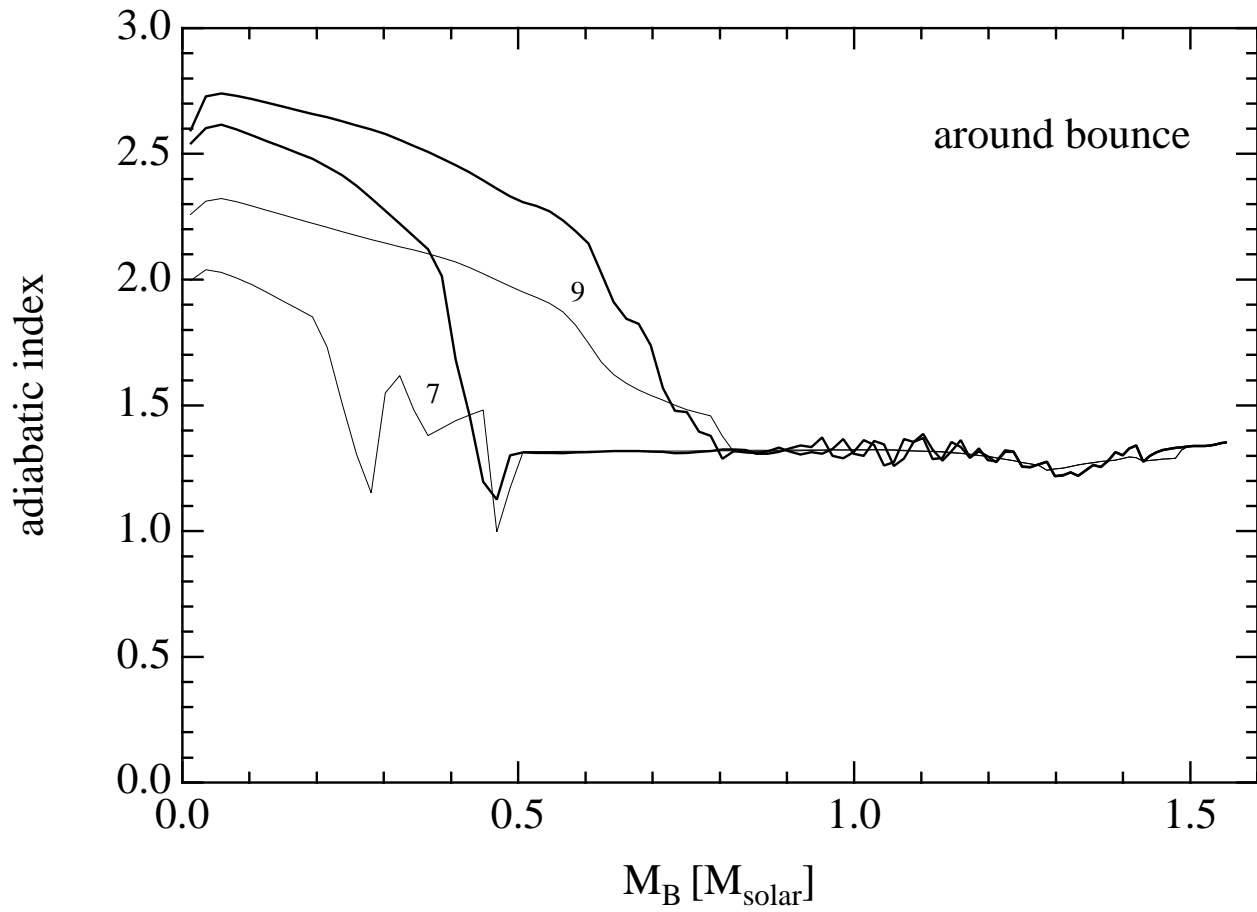


Figure 11: The adiabatic indices at around the bounce stages (7,9) are shown as a function of baryon mass coordinate for the relativistic EOS (thick) and the Lattimer-Swesty EOS (thin).



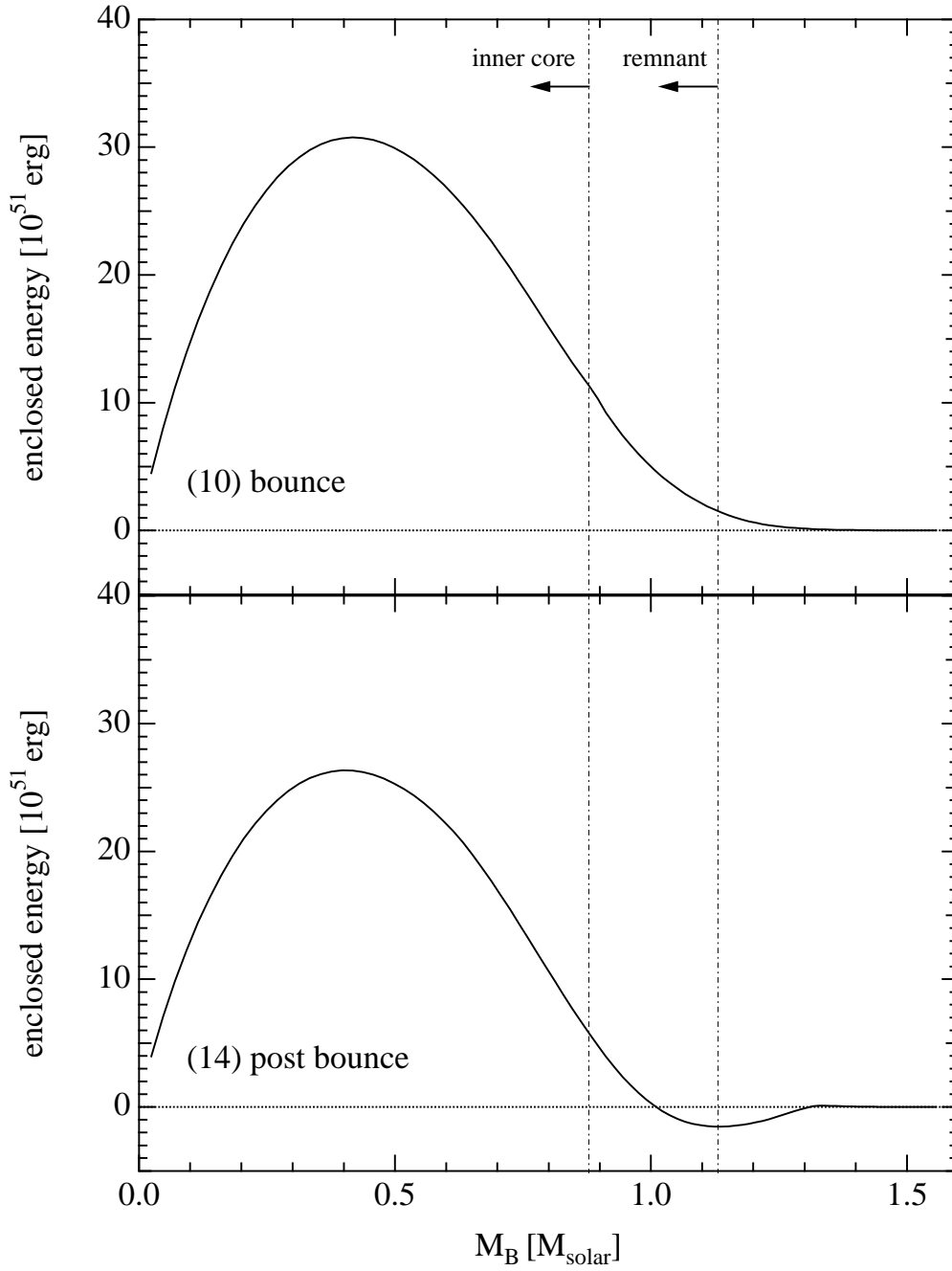


Figure 12: The profiles of the enclosed energy are shown as a function of baryon mass coordinate at the bounce stages (10,14) for the case of  $15 M_{\odot}$  model of WW95.

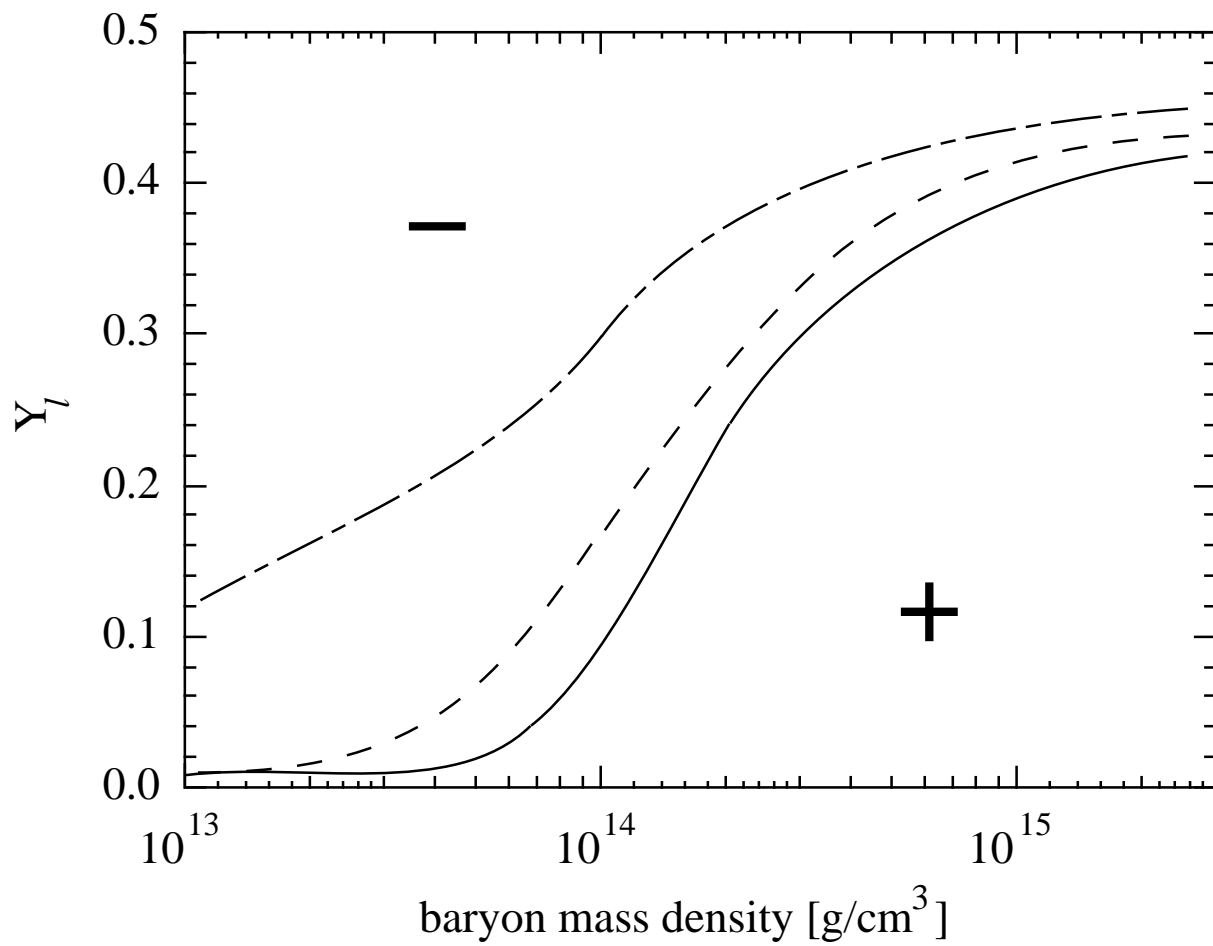


Figure 13: The sign of derivative of thermodynamical quantities, which determine convective condition, is displayed in density-lepton fraction plane. See the definition in text.